

Table 1. TDWR and 88D Radar Characteristics

TDWR and WSR-88D Technical Specifications (From NOAA/NWS Office of Science and Technology publications)		
	TDWR	WSR-88D
Transmitter		
Band	C Band	S Band
Wavelength	5.3 cm	10.5 cm
Peak Power	250 kW	750 kW
Polarization	Linear Horizontal	Dual-Pol
Maximum Reflectivity Range	460 km	460 km
Minimum Unambiguous Doppler Range	90 km	115 km
Maximum Velocity Range	90 km	230 km
Range Resolution Reflectivity	150 m (out to 135 km) 300 m (135 km – 460 km)	250 m
Range Resolution Velocity	140 m	250 m
Antenna		
Beam Width	0.55 Degrees	0.95
Power Gain	50 dB	45.5 dB
Scan Strategies		
Clear Air/Monitor Mode	Scan Time: 6 min	Scan Time: 6 – 10 min
	Number of Scans: 17	Number of Scans: 5
Severe/Hazardous Mode	Scan Time: 6 min	Scan Time: 5 min
	Number of Scans: 23	Number of Scans: 9 - 14

3. DALLAS-FORT WORTH TESTBED

As part of the National Science Foundation Engineering Research Center for Collaborative Adaptive Sensing of the Atmosphere (CASA, McLaughlin et al., 2009), the Center for Analysis and Prediction of Storms (CAPS) had developed a 400-m grid resolution real-time analysis and 1-km real-time data assimilation, nowcasting and numerical weather prediction system (NWP) using the Advanced Regional Prediction System (ARPS, Xue et al., 2001; Xue et al., 2003), and the ARPS 3D-Variational (3DVAR) and cloud analysis (Gao et al., 2004; Brewster et al., 2005; Hu et al. 2006a,b) and ran the system in a domain covering central and southwest Oklahoma (Brewster et al., 2007 and 2010).

In anticipation of the CASA radars being moved to North Texas and the establishment of an urban

testbed in the Dallas-Fort Worth (D/FW) area, the domain for this data assimilation and NWP system was relocated to the D/FW area in the spring of 2012. At the same time, thanks to cooperation among the NOAA Radar Operations Center, NWS Southern Region Headquarters and the NOAA National Severe Storms Lab, CAPS gained access to the Level-II TDWR data from the two D/FW radars. CAPS has adapted data processing code and scripts to read and process these data for the real-time NWP system and is now routinely including these data in our real-time analyses and forecasts. Interested readers can find these products online during our operational periods on the web at <http://forecast.caps.ou.edu>.

To gauge what impact these data might have in the D/FW testbed, we first examine the dual-Doppler beam crossing angles for the three Federal operational weather radars in this area, namely Fort Worth WSR-88D (KFWS) and the

TDWR radars covering Dallas Love Field (TDAL) and the Dallas-Fort Worth International Airport (TDFW). For a classic dual-Doppler analysis, a beam crossing angle between 30 and 90 degrees is considered good, with 90 degrees being ideal. Although we are not running a classic dual-Doppler analysis program, this is still a useful representation of the information content that the radars are delivering to the 3DVAR analysis, particularly when the bulk of the high resolution storm-scale wind information comes from the radars (rather than from the analysis background or other data sources).

The radar beam crossing angles in the D/FW testbed are shown in Fig 2. In this figure where the coverage of more than two radars overlap the best crossing angle of any individual pair is shown. It can be seen that the dual-Doppler crossing angles

are good throughout much of Dallas and Tarrant Counties and the southern portion of Denton County. There is a null zone, however, along the baseline connecting the three radars where the best crossing angles are less than 30 degrees. The locations of the three radars in this area happen to lie nearly along the same line. This means that in the zone southwest of Fort Worth, for example, that all the radars' viewing angles are parallel, so their measured radial velocities all reflect the same component of the wind (the strength of the southwesterly or northeasterly wind component in this case). Although the wind component measurements are duplicated in this region, the TDWR radars can provide some benefit to the 3D wind and cloud analyses by providing winds and reflectivity in the so-called "cone of silence" directly above the KFWS radar, for example.

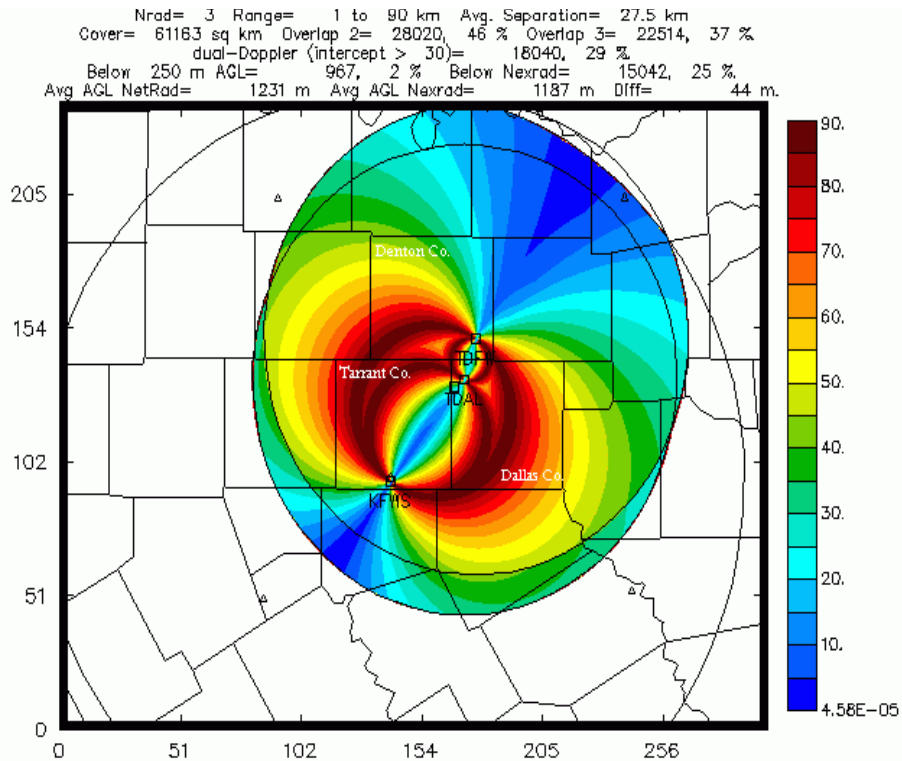


Fig 2. Dual-Doppler crossing angles (best pair) for Federal operational weather radars in the Dallas-Fort Worth area, including Fort Worth, Texas (KFWS) NEXRAD, Dallas Love Field (TDAL) TDWR and Dallas-Fort Worth International Airport (TDFW) TDWR.

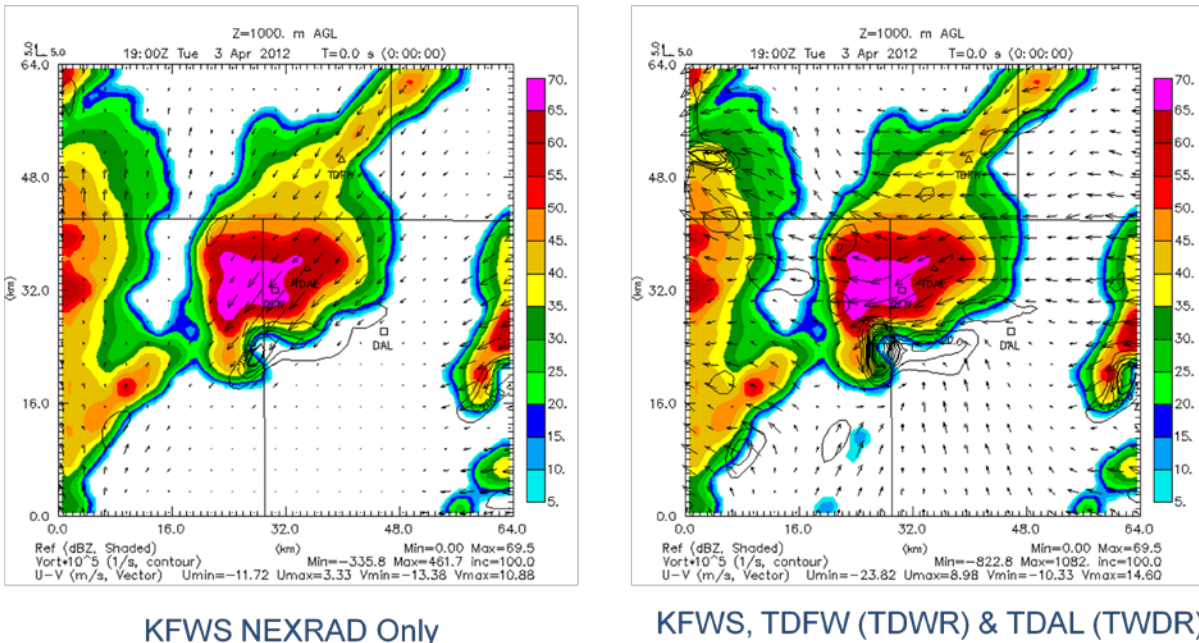


Fig 3. Comparison of CAPS 3DVAR analysis using the Fort Worth NEXRAD (KFWS) radar data only (left) and using KFWS and the two Dallas-area TDWR radars (right). Radar reflectivity (dBZ, color shading, scale at right) perturbation wind vectors (m/s, scale at upper left), and vertical vorticity (contours, $s^{-1} * 10^5$) at 1 km AGL.

4. 3 APRIL 2012 CASE

There was a severe weather outbreak in the Dallas-Fort Worth Metroplex on the afternoon of 3 April 2012. Several supercells formed in the warm sector ahead of a front west of the Dallas-Fort Worth Metroplex; other storms also formed along the front itself. The storms moved north-northeast across much of the population center and produced several damaging tornadoes and many areas of hail damage, including hail damage to aircraft at the Dallas/Fort Worth International Airport.

This case afforded the first opportunity to test the Level-II TDWR in combination with the NEXRAD radar in the CAPS 3DVAR analysis and our real-time analysis system as CAPS began receiving data shortly before April 3. Because automated software had not yet been implemented in the real-time system on that date, the forecasts presented here were run in post-real-time mode to test and demonstrate the software in the real-time configuration, which is now ready for real time use.

First we examine the impact of the TDWR on an individual 3DVAR analysis using a small test

domain with a horizontally-uniform analysis background based on the 1200 UTC Fort Worth radiosonde observation in order to clearly visualize the incremental change due to TDWR data. The domain is centered near the DFW airport, on the border between Tarrant and Dallas Counties; the locations of Dallas Love Field (DAL), Dallas-Ft. Worth International (DFW), and their respective TDWRs (TDAL and TDFW) are indicated in Fig. 3. Figure 3 shows the result of the 3DVAR and cloud analysis at 1900 UTC using the KFWS radar in the left frame and, in the right frame, the result after adding the TDWR data from TDAL and TDFW. Shown are the model-based reflectivity, the perturbation velocity vectors (difference from the uniform horizontal mean wind) and the vertical vorticity (positive values contoured). There is only a small difference in reflectivity, as the region is relatively close to the KFWS radar (which is located just outside the domain to the southwest), and the algorithms for determining the hydrometeors use a maximum-value mosaic among all the radar observations covering any individual grid cell. In the wind fields the vertical vorticity maximum near the hook echo of the hailstorm near the DFW airport is increased from $4.61 \times 10^{-3} s^{-1}$ to $10.62 \times 10^{-3} s^{-1}$ as data from the TDWRs help to better define the circulation there.

NEXRAD does not report radial wind in the “clear air” regions having reflectivity less than 0 dBZ while operating in storm mode, but TDWR does provide some information in those regions so the wind fields to the south and east of the supercell are updated with data from TDAL and TDFW, both showing inflow into the cell. Also, the addition of TDWR data shows inflow into the convection on the western edge of the domain perpendicular to the KFWS beam.

Results of the assimilation and NWP experiment at 1800 UTC are shown Fig. 4. As in the real-time forecasts, the most-recent NAM 12-km forecast is used here as the analysis background and for boundary conditions. In the figure the first column has the results using NEXRAD radar data, surface observations, and other conventional data, the middle column is the result after adding TDWR data, and the right column shows the verifying low-level (0.5° elevation) radar scan from the Fort Worth (KFWS) NEXRAD.

Two 5-minute assimilation cycles of the ARPS 3DVAR and incremental analysis updating (IAU, Bloom et al., 1996) are used in this assimilation experiment, so the first row shows the result at 1800 UTC, after the 10-minute data assimilation period (1750-1800 UTC), the second row shows the results after the second data assimilation cycle (1800-1810 UTC), the third row is 25 minutes of forecasting (5 minutes beyond the end of the second assimilation period), and the last row is after 40 minutes of forecasting (1830 UTC). Of the two supercells in the center of the domain, the model handles the eastern cell better, more accurately predicting its strength and motion. The western cell, the cell that produced hail that impacted the Dallas-Fort Worth International Airport, is initialized almost directly over the KFWS NEXRAD radar. This is not an ideal location due to the so-called “cone of silence” for the KFWS radar data directly above the radar site caused by the fact that the radar scans only to 19.5° elevation angle so it is blind to what is occurring directly overhead. The assimilation process and the addition of radar data from other radars can help that situation as we see in the second column, where the addition of the TDWR results in a forecast with a stronger cell that has a position that more closely matches the observed radar, has better reflectivity and more low-level rotation at 18:15 and 18:30 UTC.

5. DIFFERENCE FIELDS

In order to more clearly see the impact of the TDWR radar data on the forecasts, difference fields are created subtracting the analyses and forecasts using all the radar data from the parallel analyses and forecasts excluding the TDWR radar data. Figure 5 shows the difference vectors in the 3DVAR analysis at 1-km AGL at the initial time (nominal time 1750 UTC, data in the window 1750-1800), and the differences at the end of the 10-min IAU window ending at 1800 UTC (right panel). The magnitudes of the wind differences are up to 9.9 ms^{-1} in the u component and 6.2 ms^{-1} in the v component. Most of the differences are within the two isolated supercells and in a portion of the squall line to the west of Fort Worth. Notable are v-component differences in the eastern supercell and northeasterly wind differences in the squall line northwest of KFWS radar, both of which are perpendicular to the Fort Worth radar beam in those areas.

After the 10-minute IAU period most of the differences have been retained, with some small reduction in magnitude (up to 9.4 ms^{-1} in u and 4.1 ms^{-1} in v), and there are some perturbations to the differences likely due to the precipitation differences in the storms interacting with the wind field changes at this level.

Figure 6 shows the differences in the second cycle 3DVAR analysis (nominal time 1800 UTC, data from 1800-1810) and in the ARPS forecast at the end of the IAU assimilation window at 1810 UTC (left panel). Similar to the first cycle analysis, the TDWR radars introduce differences in the two supercells and in the squall line northwest of the KFWS radar. The magnitudes of the differences are up to 6.9 ms^{-1} in the u component and 6.4 ms^{-1} in the v component. The differences here extend into some of the non-precipitating areas, more so than in the first cycle. As with the first cycle most of the differences are retained after assimilation of the analysis fields into the model. After assimilation, the magnitudes are up to 10.5 ms^{-1} in u component and 7.0 in the v component with the majority of the changes in the analysis being retained, plus some additional strength in the outflow of the squall line on the east edge of the squall line northwest of KFWS, likely due to precipitation differences in this area.

Figure 7 shows the vector wind differences at the 1-km AGL level for the forecasts valid at 1815 UTC (left panel) and 1830 UTC (right). There is growth in the magnitudes of the maximum differences with time as non-linear effects and differences in position evolve over time. Of interest is a cyclonic circulation in the difference field in the western supercell as the net effect of the addition of TDWR data increases the low-level rotation in this cell.

Also presented are differences calculated between a model run using all radars except one of the TDWR radars, TDAL, in other words showing the effect due to just adding TDAL. Figures 8-10 show these results in the same way the difference results were shown in Figures 5-7. Not surprisingly, the magnitudes of the differences from just adding TDAL are smaller than the differences due to adding both radars. For example, it appears that much of the difference in the eastern supercell at this level was due to observations from TDAL, which is closer to this cell. Similar to the result in Fig. 5, we see in the right panel of Fig. 8 that most of the changes in the analysis are retained after the IAU assimilation period, with maximum differences about 20% less in the assimilated field than the analysis. The results for the second cycle (Fig 9) and then in the subsequent forecast (Fig 10) follow the result seen in the difference fields from both radars, except the magnitudes are decreased by the lack of data from TDAL. For example there is only a small increase in cyclonic circulation at this level in the western supercell.

6. OTHER TDWR-RICH LOCATIONS

The D/FW location is somewhat unusual in having two TDWR radars located in the same metropolitan area, but this characteristic is not unique. Based on the distribution of radars apparent in Fig 1, we considered some of the other regions that have closely-spaced TDWRs and NEXRAD radars and we calculated dual-Doppler beam crossing angles for two other TDWR-rich areas.

Results of these analyses are shown in Fig 11 and Fig 12 for the Washington, DC area and the South Florida area, respectively. The Washington, DC area is especially rich with Federal operational weather radars. The three civilian airports serving Washington and Baltimore, namely Dulles International, Ronald Reagan National, and Baltimore/Washington International-Thurgood Marshall, are covered by TDWR radars, as well as Andrews Air Force Base. The combination of these TDWR radars with the NEXRAD radars in the area provides a broad area with excellent dual-Doppler crossing angle covering the District of Columbia, much of eastern Virginia, Eastern Maryland, Chesapeake Bay, and parts of Delaware.

In South Florida the TDWRs covering Miami International, Fort Lauderdale/Hollywood and Palm Beach International airports form a line of dense radars. When combined with the NEXRAD data there is good dual-Doppler coverage along the coast from Biscayne Bay to West Palm Beach, and, similarly, in a corridor of South-Central Florida west of the line of radars.

These locations and other locations have great opportunity for analysis and forecast improvement using TDWR data. Although CAPS does not have real-time access to Level-II TDWR data for these sites, CAPS will investigate using the more-commonly available Level-III TDWR data (with slightly degraded velocity and reflectivity descritization compared to Level-II) for CAPS real-time experiments, such as the Spring Storm Scale Ensemble Experiment (e.g. Clark et al. 2011) which cover the entire Continental United States.

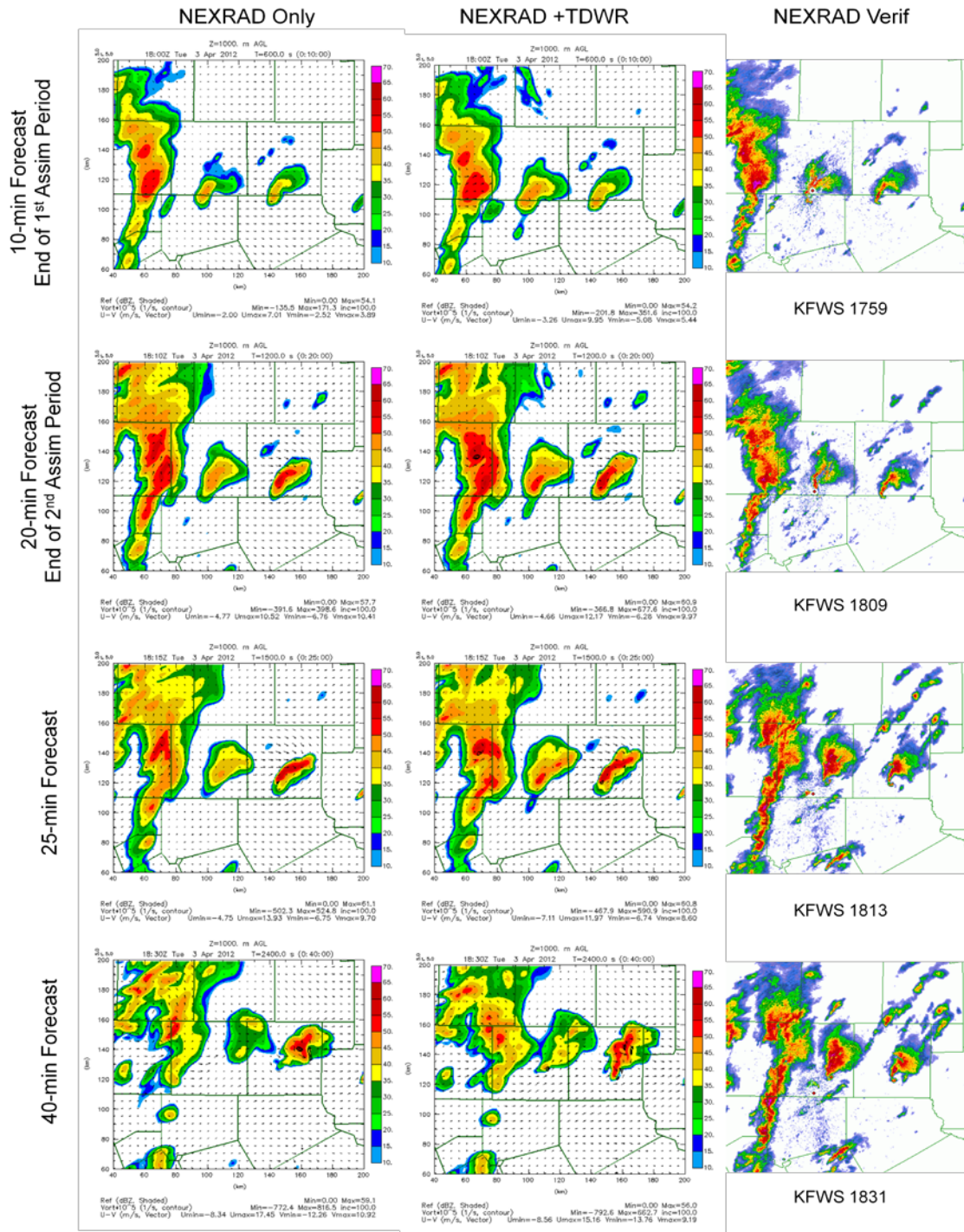


Fig 4. Data assimilation and forecast results for 3 April 2012. Left column: Model result at 1-km AGL using only NEXRAD, surface and other conventional data, model radar reflectivity estimate (dBZ, colors), horizontal wind vectors (scale at upper-left), and vertical vorticity (positive values, contours). Center column, same as left, adding TDWR data to the analysis and assimilation. Right column, verifying NEXRAD radar reflectivity, 0.5 degree reflectivity (dBZ). First row: After 10 minutes of assimilation (1800 UTC), Second Row: end of second data assimilation cycle (1810), Third row: 25 minute forecast (1815), Fourth Row: 40-min forecast (1830).

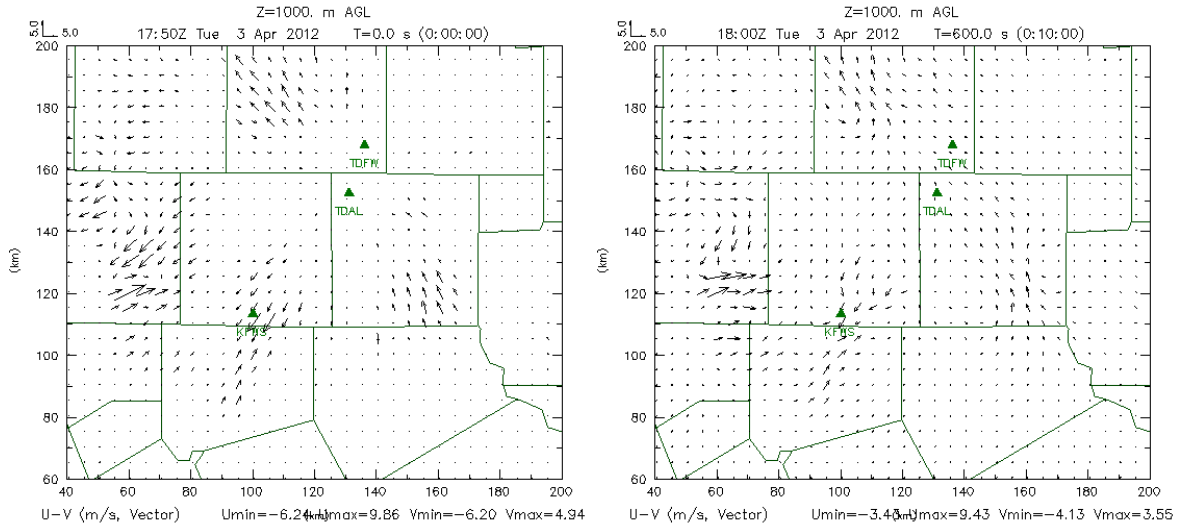


Fig 5 1-km AGL wind vector difference fields, all-data run minus the run without TDWR radars. Left: Initial 3DVAR analysis for 1800 UTC. Right: ARPS model forecast at 1800 UTC, end of 10-min IAU window.

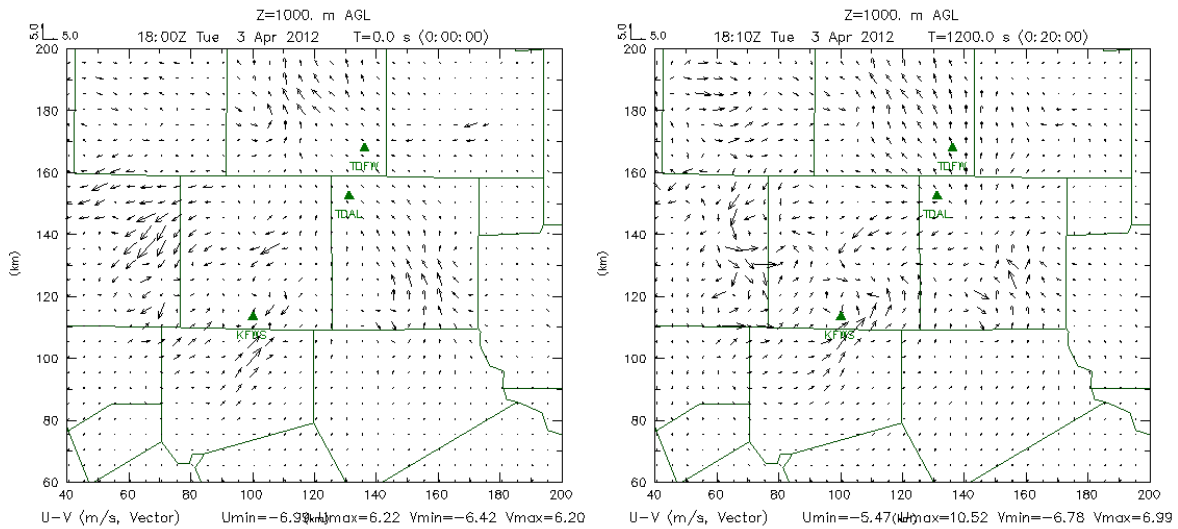


Fig 6 1-km AGL wind vector difference fields, all-data run minus the run without TDWR radars. Left: Second cycle 3DVAR analysis. Right: ARPS model forecast at 20-min, end of second IAU window.

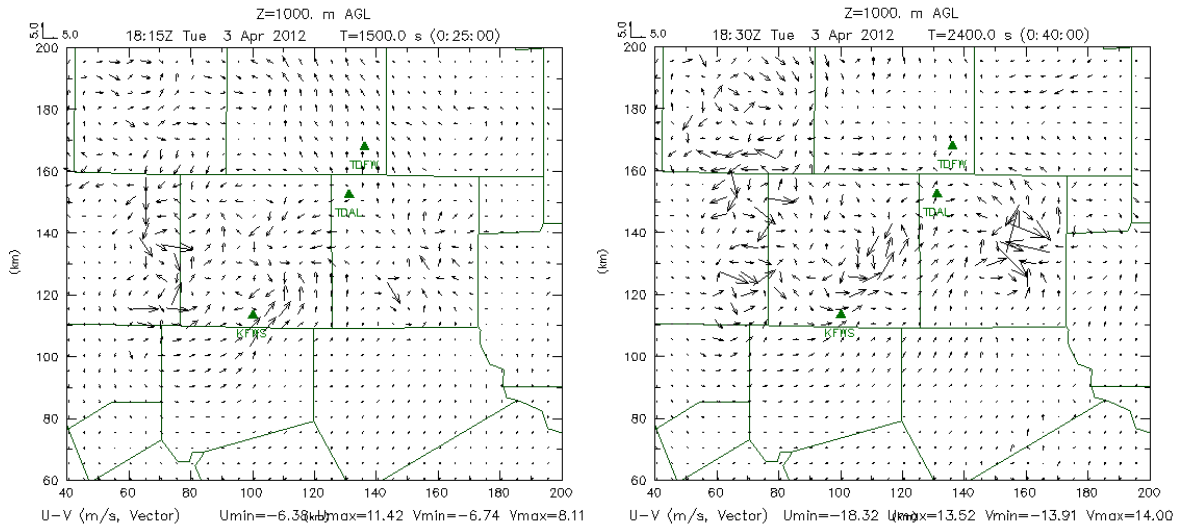


Fig. 7 1-km AGL wind vector difference fields, all-data ARPS forecast minus the ARPS forecast without TDWR radars. Left: 1815 UTC. Right: 1830 UTC.

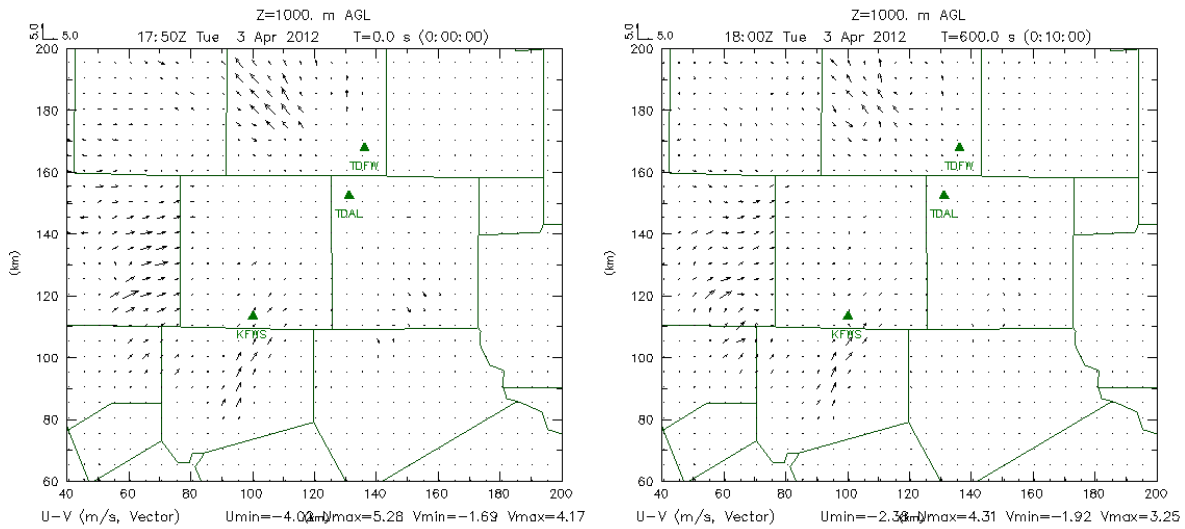


Fig. 8 1-km AGL wind vector difference fields, all-data run minus the run without the Dallas Love Field TDWR radar (TDAL). Left: Initial 3DVAR analysis. Right: ARPS model forecast at 10-min, end of IAU window.

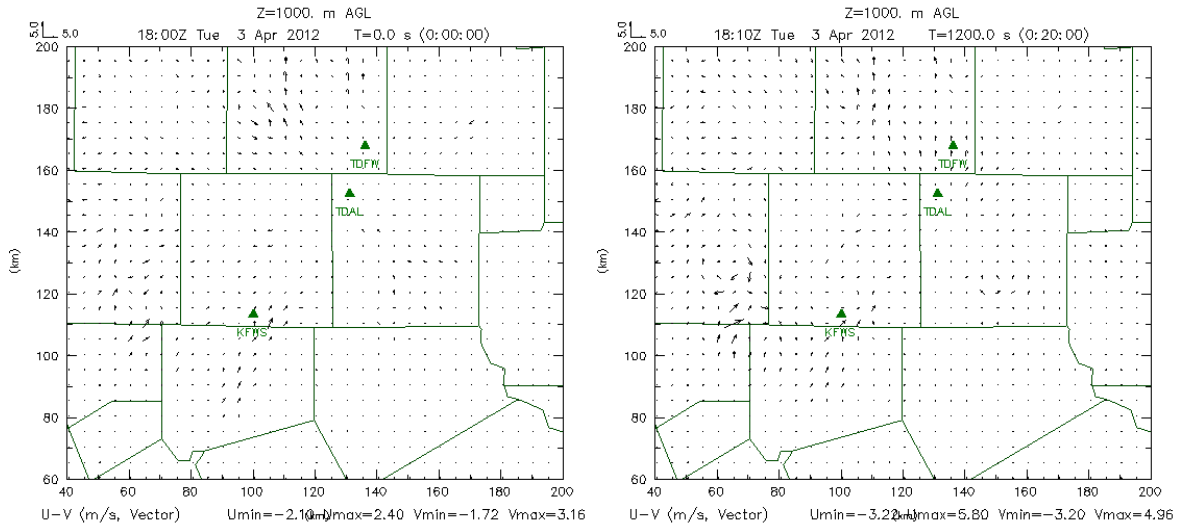


Fig. 9 1-km AGL wind vector difference fields, all-data run minus the run without TDWR radars. Left: Second cycle 3DVAR analysis. Right: ARPS model forecast at 20-min, end of second IAU window.

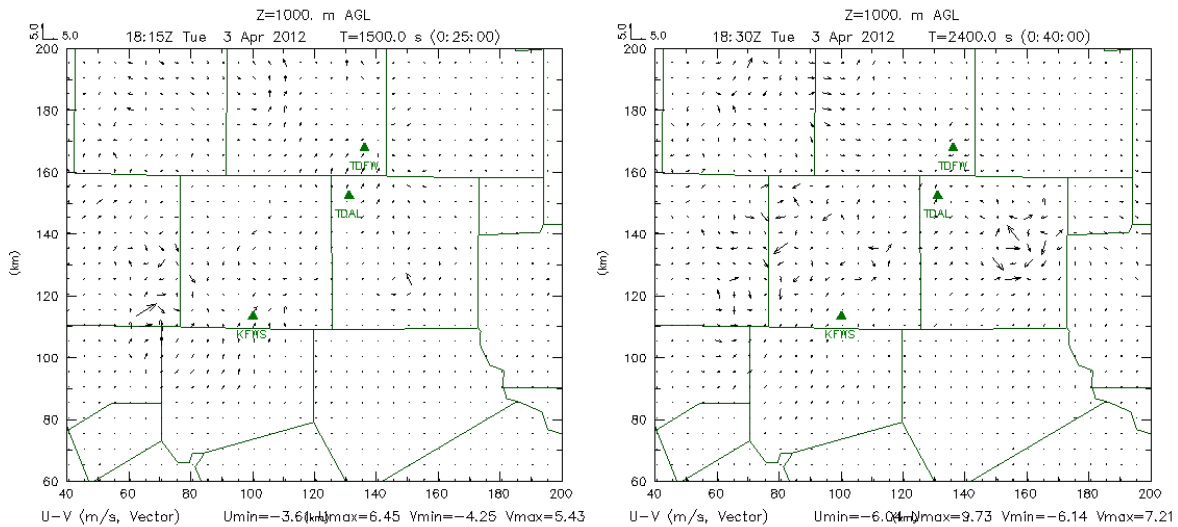


Fig. 10 1-km AGL wind vector difference fields, all-data ARPS forecast minus the ARPS forecast without TDWR radars. Left: 1815 UTC. Right: 1830 UTC.

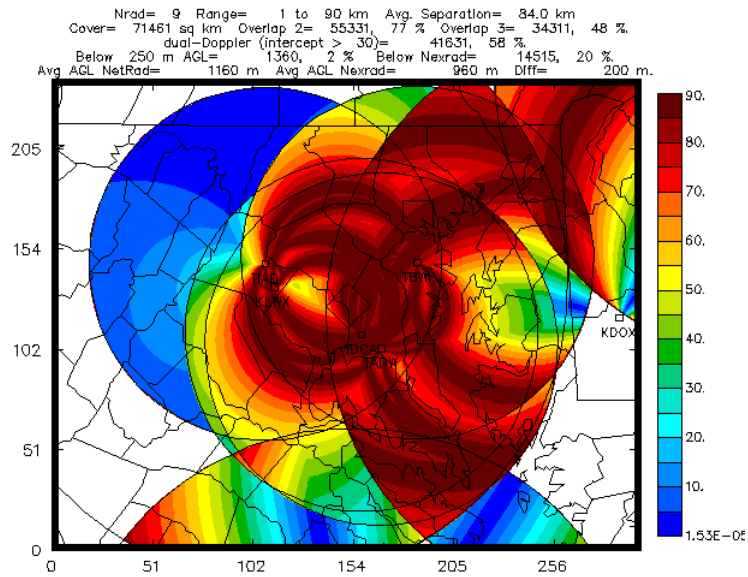


Fig 11 Radar beam crossing angles (degrees) in the Washington, DC area. NEXRAD radars: Sterling, Virginia (KLWX), Dover Air Force Base, Delaware (KDOX), Norfolk, Virginia (KAKQ), Mount Holly, New Jersey (KDIX), State College, Pennsylvania (KCCX), TDWRs: Andrews Air Force Base (TADW), Baltimore/Washington International (TBWI), Reagan National Airport (TDCA), Dulles International (TIAD).

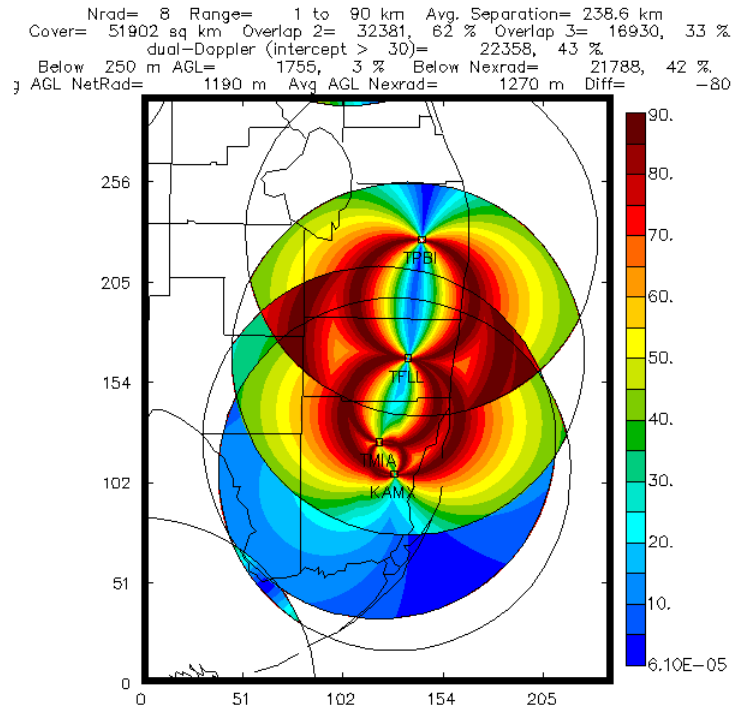


Fig. 12 Radar beam crossing angles in Southeast Florida. NEXRAD radars Key West (KBYX), Miami (KAMX), and Melbourne (KMLB), and TDWRs: Miami International (TMIA), Fort Lauderdale/Hollywood (TFL) and Palm Beach International (TPBI).

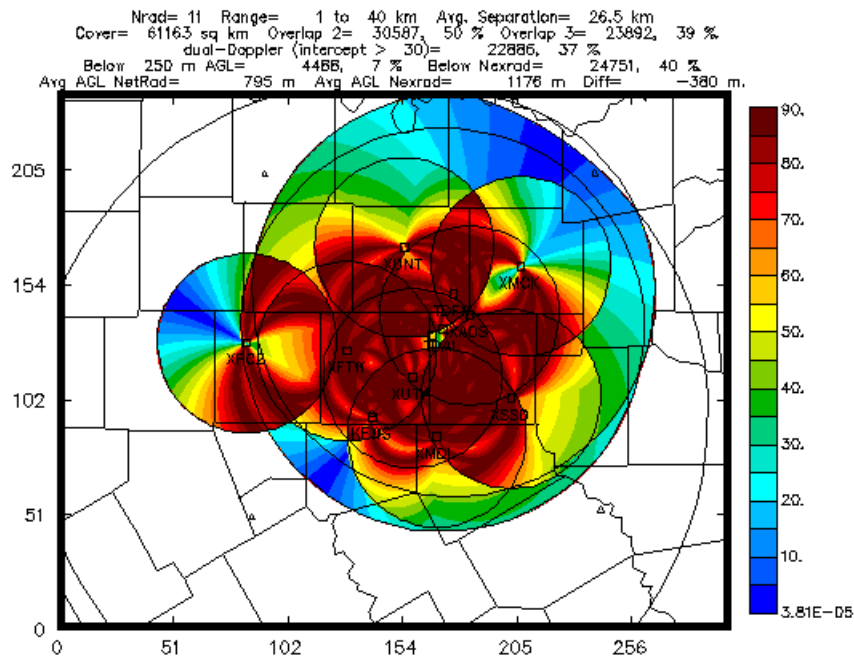


Fig. 13. Radar beam crossing angles for the combination of NEXRAD radars, TDWRs, and a proposed set of locations for CASA X-band research radars in the Dallas-Fort Worth metro area. NEXRAD: Fort Worth, Texas (KFWS), TDWR: Dallas Love Field (TDAL) and Dallas-Fort Worth International Airport (DFW), CASA: Arlington, Denton, Fort Worth, Addison, Southeast Dallas, Midlothian, McKinney, and Weatherford, Texas.

7. SUMMARY AND CONCLUSIONS

Level-II data from TDWR radars in the Dallas-Fort Worth Metroplex have been successfully added to the CAPS real-time analysis and forecast system for the D/FW Testbed. We shown a positive impact from adding these new data in this region for one test case. Other areas where addition of TDWR radars in combination with NEXRAD data are expected to produce high-quality 3D wind analyses and subsequent nowcasts and short-term forecasts have been shown.

CASA X-band radars with a nominal range of 40-km are being added to the D/FW testbed. To date four sites have been identified which will be the new locations for the four CASA X-band radars which had been located in southwestern Oklahoma. There are four new X-band radars that will be available for the D/FW testbed so it is of interest to explore the dual-Doppler beam

crossing angles for configurations of the 8-radar X-band network, including the four known sites, in order to decide on the best locations for the remaining sites. Figure 13 shows the beam crossing angles for the 11-radar network formed by the combination of the Federal radars and CASA radars in one possible configuration of the 8-radar CASA network.

It should be noted that the final decision on radar siting will depend on a number of other factors including improving the low-level coverage of radar over the D/FW Metroplex (which favors locations distant from KFWS, in the northeast portion of this domain), improving the upstream data coverate, local terrain, and the availability of suitable host locations with necessary power and communications bandwidth, as was done for determining the sites for the CASA radar network in Oklahoma (Brewster et al., 2005).

8. ACKNOWLEDGMENTS

The authors would like to thank ROC staff, particularly Tim Crum, and Karen Cooper of NSSL for their help in gaining access to the real-time Level-II TDWR data for the D/FW testbed.

The D/FW Testbed and CASA work is supported in part by the National Science Foundation (NSF) under EEC03-13747, by the NWS, and the North Central Texas Council of Governments. Any opinions, findings, conclusions, or recommendations expressed in this material are those of the authors and do not necessarily reflect those of the funding agencies. Supercomputing resources from the Oklahoma University Supercomputing Center for Education and Research (OSCE) were used for the analyses and forecasts in this study.

9. REFERENCES

- Bloom, S. C., L. L. Takacs, A. M. da Silva, D. Ledvina, 1996: Data Assimilation Using Incremental Analysis Updates. *Mon. Wea. Rev.*, **124**, 1256–1271.
- Brewster, K., L. White, B. Johnson, and J. Brotzge, 2005: Selecting the sites for CASA NetRad, a collaborative radar network. Ninth Symposium on Integrated Observing and Assimilation Systems for the Atmosphere, Oceans and Land Surface (IOAS-AOLS), 85th Amer. Meteor. Soc. Annual Meeting CD, Paper: P3.4.
- Brewster, K., M. Hu, M. Xue, and J. Gao, 2005: Efficient assimilation of radar data at high resolution for short range numerical weather prediction. World Weather Research Program Symposium and Nowcasting and Very Short-Range Forecasting WSN05, Toulouse, France. WMO World Weather Research Program, Geneva, Switzerland. Symposium CD, Paper 3.06.
- Brewster, K.A., K. W. Thomas, J. Brotzge, Y. Wang, D. Weber, and M. Xue, 2007: High resolution assimilation of CASA X-band and NEXRAD radar data for thunderstorm forecasting. 22nd Conf. Wea. Anal. Forecasting/18th Conf. Num. Wea. Pred., Salt Lake City, Utah, Amer. Meteor. Soc., Paper 1B.1
- Brewster, K., K. Thomas, J. Gao, J. Brotzge, M. Xue, and Y. Wang, 2010: A nowcasting system using full physics numerical weather prediction initialized with CASA and NEXRAD radar data. Preprints, 25th Conf. Severe Local Storms, Denver, CO, Amer. Meteor. Soc., Denver, CO, Paper 9.4.
- Gao, J., M. Xue, K. Brewster, and K. K. Droegemeier 2004: A three-dimensional variational data assimilation method with recursive filter for single-Doppler radar, *J. Atmos. Oceanic. Technol.* 457-469.
- Hu, M., M. Xue, and K. Brewster, 2006a: 3DVAR and cloud analysis with WSR-88D Level-II Data for the Prediction of Fort Worth Tornadoic Thunderstorms Part I: Cloud analysis and its impact. *Mon. Wea. Rev.*, **134**, 675-698.
- Hu, M., M. Xue, J. Gao and K. Brewster: 2006b: 3DVAR and Cloud Analysis with WSR-88D Level-II Data for the Prediction of Fort Worth Tornadoic Thunderstorms Part II: Impact of radial velocity analysis via 3DVAR, *Mon Wea Rev.*, **134**, 699-721.
- Istok, M.J., A.D. Stern, R.E. Saffle, B. Bumgarner, B.R. Klein, N. Shen, Y. Song, Z. Wang, and W.M. Blanchard, 2008: Terminal Doppler Weather Radar for NWS Operations: Phase 3 Update. 24th Conf on Interactive Information and Processing Systems (IIPS), Amer. Met. Soc., Paper 6B.10.
- Xue, M., K. K. Droegemeier, V. Wong, A. Shapiro, K. Brewster, F. Carr, D. Weber, Y. Liu, and D.-H. Wang, 2001: The Advanced Regional Prediction System (ARPS) - A multiscale nonhydrostatic atmospheric simulation and prediction tool. Part II: Model physics and applications. *Meteor. Atmos. Physics*, **76**, 143-165.
- Xue, M., D.-H. Wang, J. Gao, K. Brewster, and K.K. Droegemeier, 2003: The Advanced Regional Prediction System (ARPS) – storm-scale numerical weather prediction and data assimilation. *Meteor. Atmos. Physics*, **82**, 139-170.